Modulated structure of Rb_2ZnCl_4 in the soliton regime close to the lock-in phase transition

I. Aramburu,[1,*] K. Friese,[2] J. M. Pérez-Mato,[2] W. Morgenroth,[3] M. Aroyo,[2] T. Breczewski,[4] and G. Madariaga[2]

[1]*Departamento de Física Aplicada I, Escuela Superior de Ingenieros de Bilbao, Universidad del País Vasco, Alda. Urquijo s/n, 48013 Bilbao, Spain*

[2]*Departamento de Física de la Materia Condensada, Facultad de Ciencia y Tecnología, Universidad del País Vasco, Apartado 644, 48080 Bilbao, Spain*

[3]*Hamburger Synchrotronstrahlungslabor am DESY, Notkestrasse 85, 22603 Hamburg, Germany*

[4]*Departamento de Física Aplicada II, Facultad de Ciencia y Tecnología, Universidad del País Vasco, Apartado 644, 48080 Bilbao, Spain*

(Received 5 August 2005; revised manuscript received 7 November 2005; published 24 January 2006)

The structure of the incommensurate phase of Rb_2ZnCl_4 has been determined at 194 K (2 K above the lock-in transition) within the soliton regime using satellites up to fifth order. The rather anharmonic modulation functions agree with the expected steplike functions supported by theoretical arguments. In addition, the constancy of the ratio between the amplitudes of the fifth-order and first-order harmonics, a relation predicted by theory, indicate the correctness of the model and imply a value of 0.4 for the soliton density n_s. A symmetry mode analysis shows that the incommensurate structure is consistent with the one of the lock-in phase in the sense that the displacement pattern of every symmetry mode remains unaltered in the transition except for a global change in the amplitudes.

DOI: 10.1103/PhysRevB.73.014112 PACS number(s): 64.70.Rh, 61.10.Nz, 61.44.Fw, 64.70.Kb

I. INTRODUCTION

Incommensurately modulated phases with a one-dimensional modulation are often thermally stabilized in a temperature range limited by two commensurate phases, a high-temperature (parent) nonmodulated phase at T_i, and a low-temperature "lock-in" phase at T_L. At this latter temperature the varying modulation wave vector $\mathbf{q}$ of the incommensurate phase locks into a rational value $\mathbf{q_L}$ (Refs. 1–3). In one of the simplest and most common situations, the lock-in and incommensurate wave vectors lie on a symmetry line of the Brillouin zone and the order parameter is two-dimensional. In such cases, according to a generalized Landau theory,[1,4] the order parameter can be considered a complex quantity $Q=\rho\exp(i\,2\pi\theta)$, representing the complex amplitude of the primary distorting mode in the lock-in phase. The incommensurate phase is then described by a space-dependent order parameter $Q(z)$ along the direction of the wave vector. The corresponding Landau potential predicts that, as temperature decreases, the structure of the incommensurate phase is driven continuously from an initial sinusoidal configuration close to the parent-incommensurate transition into a strongly anharmonic modulation, the so-called soliton regime, previous to the lock-in phase transition. In this soliton regime the modulation is steplike, with regions where the order parameter is approximately constant (i.e., nanodomains approximately commensurate corresponding to the lock-in phase) separated by coherent periodic "discommensurations," where the phase $\theta(z)$ of the complex order parameter varies rapidly to the next approximately constant value (see Fig. 1). In the simplest approximation this steplike behavior of the phase $\theta(z)$ satisfies the sine-Gordon equation.[4] The density along z of discommensurations, the so-called soliton density (n_s), can be taken as an order parameter with respect to the lock-in phase. A zero soliton density would correspond to the lock-in phase while $n_s=1$ is associated to the sinusoidal modulation.[5] In general the incommensurate configuration approaches the configuration corresponding to the lock-in phase in two ways: (i) by varying the incommensurate modulation wave vector $\mathbf{q}$ so that it approaches the commensurate value $\mathbf{q_L}$ and (ii) by progressively transforming the structural modulation from a sinusoidal to a steplike function corresponding to $n_s=0$. The lock-in phase transition has, however, a discontinuous character and takes place before either the modulation wave vector or the soliton density reach their limiting values.

The soliton regime has been observed in simulations with microscopic models[6,7] and has been confirmed experimentally in various incommensurate materials by several techniques. Soliton regimes with soliton densities as low as 0.2 have been reported.[8] In numerical simulations the discontinuity of the lock-in phase transition appears to be related with a break of analyticity of the structural modulations before reaching the ideal steplike form.[7]

Although the existence of a soliton regime as a precursor of a lock-in phase has been evidenced experimentally in many incommensurate systems by means of various spectroscopic techniques and electron microscopy,[5,8–12] a rigorous determination of the corresponding modulated structures in this highly anharmonic regime by means of diffraction experiments has not been reported up to now. This means that the various very restrictive properties of the atomic structural modulation, either assumed or predicted by the Landau theory, have not been properly cross-checked experimentally. Only in cases, as thiourea[13] or BCCD,[14] where the atomic modulations have only two steps, and the role of higher harmonics is rather limited, a proper structure determination within some kind of soliton regime has been reported. These compounds are however not valid as examples for the "canonical" soliton regime with a single two-dimensional order parameter. In these materials the lock-in wave vector is at the center of the Brillouin zone and the order parameter of the lock-in phase is one dimensional. This implies that the mode

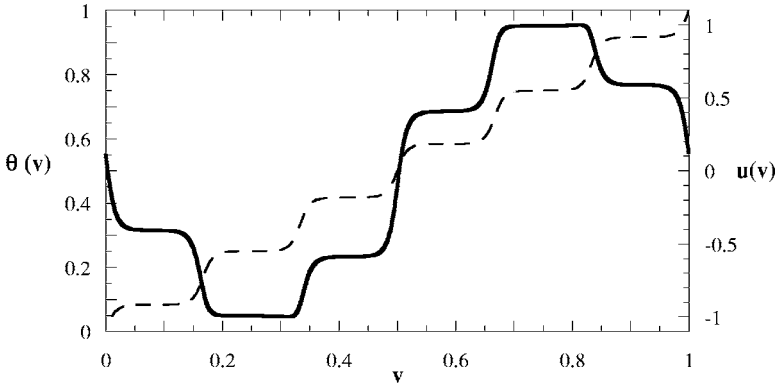

FIG. 1. Discontinuous line: Scheme of the space variation of the phase θ of the complex order parameter in an incommensurate phase with a soliton density $n_s=0.2$ and six types of domains, as obtained from the sine-Gordon equation. Continuous line: Example of the corresponding modulation of an atomic position $u(v)$ in arbitrary units. Both functions are represented along the internal coordinate v of the superspace description. A lattice point in real space $\mathbf{l}$ has an internal coordinate value $v=\mathbf{q}\cdot\mathbf{l}$ (mod. 1).

eigenvector of the incommensurate distortion strongly changes as the wave vector approaches the lock-in transition, a situation outside the implicit assumptions of the standard description of the soliton regime in incommensurate systems.[15]

Rubidium tetrachlorozincate Rb_2ZnCl_4, on the other hand, is an archetypical example of an incommensurate system where a Landau free energy with a two-dimensional order parameter can be defined, and a soliton regime is expected before the lock-in transition. This compound is in fact one of the most studied materials having an incommensurate phase. Its stability range is limited by the temperatures $T_i \approx 303$ K and $T_L \approx 192$ K. In a setting where the parent phase has symmetry *Pmcn* the modulation wave vector of the incommensurate phase is $\mathbf{q}=\left[\frac{1}{3}-\delta(T)\right]\mathbf{c}^*$, while the modulation wave vector of the lock-in phase is $\mathbf{q_L}=\frac{1}{3}\mathbf{c}^*$, i.e., the lock phase is a threefold superstructure along the c axis. The expected soliton regime of Rb_2ZnCl_4 has been observed in numerous experimental studies.[10,16–19] However, as in other similar compounds, diffraction studies have only arrived to propose quantitative structural models for the incommensurate phase limited to sinusoidal modulations.[20,21] Moreover, some authors have even argued that the diffraction diagram of Rb_2ZnCl_4 is not consistent with the soliton regime description.[22]

The difficulty of observing and analyzing quantitatively by means of diffraction techniques the anharmonic atomic modulations expected in the soliton regime as the one represented in Fig. 1, is due to the fact that the main signature of this "well-structured" anharmonicity locates in rather high-order diffraction satellites. In the case of Rb_2ZnCl_4, the number of steps for the order parameter phase, and consequently in the atomic modulation functions, is 6 as represented in Fig. 1. This number is associated with the number of twin and antiphase domains in the lock-in phase. For such six-step atomic modulation functions, the Fourier decomposition contains only harmonics of order $\{1,6n\pm1\}(n\in Z^+)$, so that fifth-order and seventh-order Fourier terms are the first relevant terms, and diffraction satellites of these orders should be the main signature of the solitonic shape of the atomic modulation functions. But even in the most anharmonic regime, in the case of $n_s=0$, when the functions in Fig. 1 become perfect steplike functions, the intensity ratio of fifth-order and seventh-order satellites with respect to first-order ones are expected to reach values of the order of $1/5^2$ and $1/7^2$, respectively.[23] Considering that first-order satellites are typically one or two orders of magnitude weaker than the main reflections, corresponding to the average structure, a proper quantitative determination of these soliton modulated structures requires to obtain and analyze datasets with intensities over a range of at least three orders of magnitude where the ones significant for determining the soliton features in the atomic modulation functions are the weakest. Furthermore, these high-order satellite peaks superimpose with first-order satellites at the lock-in transition, and therefore, in the soliton regime, near to the transition, they are usually so close that problems for resolving them can occur.

A conspicuously high relative intensity of fifth-order and seventh-order satellites in Rb_2ZnCl_4 could already be observed in the earlier results reported by Andrews *et al.*[24] Subsequently, in Ref. 25 a thorough study of the temperature variation of a limited set of satellites up to the seventh order measured with a rotating anode x-ray source was reported and shown to be consistent with the existence of a soliton regime as described by the Landau functional. More recently Babkevich *et al.*[22] based on another set of measurements claimed rather opposite conclusions. This latter study is, however, invalidated because the authors erroneously assumed soliton functions with three steps, instead of the six which are appropriate for Rb_2ZnCl_4. Unfortunately this error seems to be propagating in more recent publications.[26]

The effect of a soliton regime on the diffraction diagram of Rb_2ZnCl_4 was analyzed theoretically and simulated by Aramburu *et al.*[27] It was shown that, if the effect of secondary modes is neglected, the ratio of the intensities of pairs of fifth-order and first-order satellites superimposing at the lock-in transition will follow a unique law, dependent only on the soliton density n_s and independent of the specific reflection. A simulation showed that secondary modulations not associated with the order parameter may produce a significant dispersion of these intensity ratios, but their mean value did not change and could still be related with the theoretical value dependent only on n_s. Accordingly, the measurement of these intensity ratios was proposed as a method for determining the soliton density in the structure.

In this paper, we report a full structure determination of the incommensurate structure of Rb_2ZnCl_4 at 194 K, approximately 2 K above the lock-in phase transition, where a soliton regime is expected. Satellites up to the fifth order have been included in the dataset, and all atomic modulation functions have been refined including Fourier harmonics up to this order. A thorough comparison of both the fitted struc-

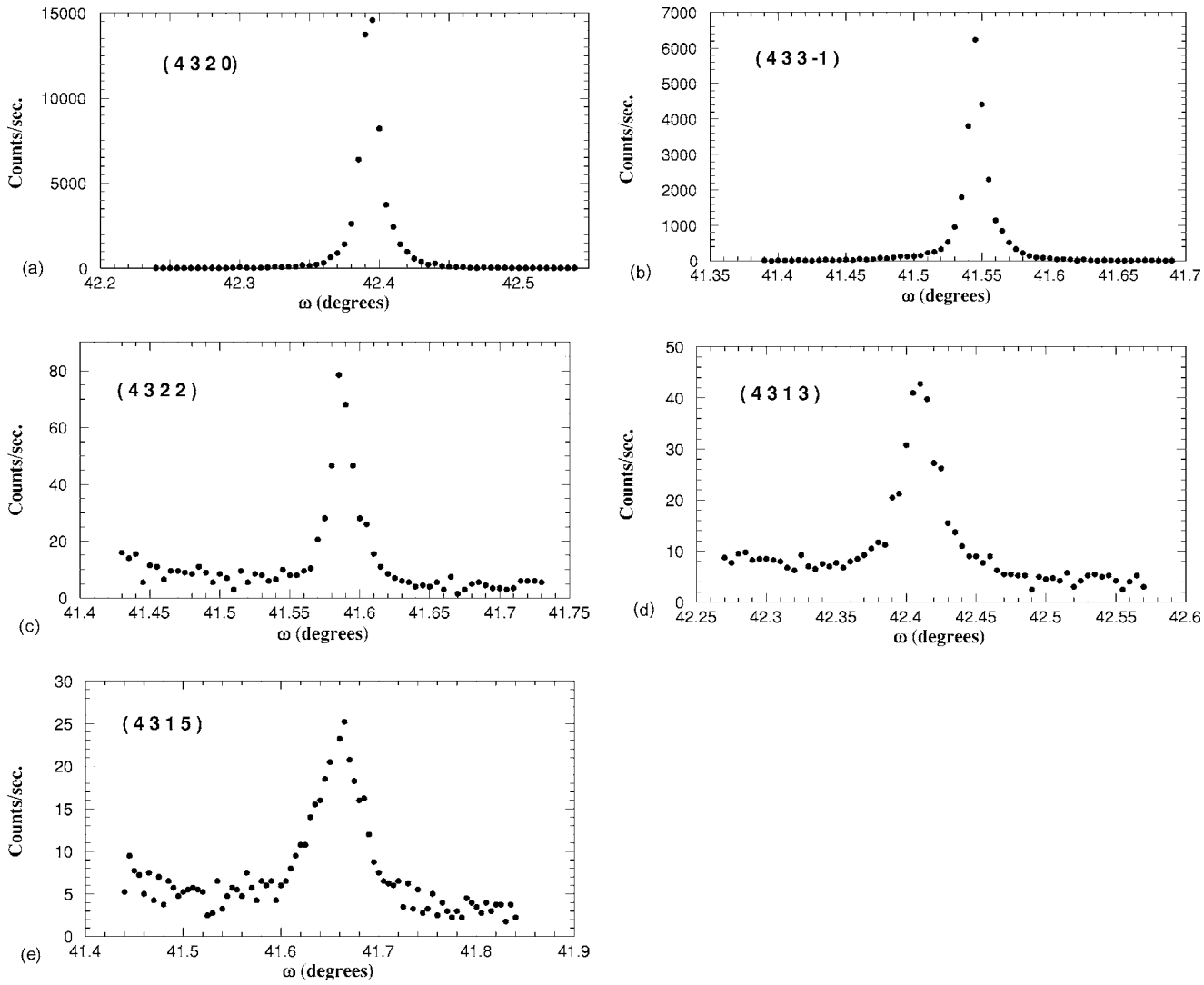

FIG. 2. Representative profiles of the (a) main reflection (4,3,2,0) and the satellite reflections (b) $(4,3,3,-1)$, (c) (4,3,2,2), (d) (4,3,1,3), and (e) (4,3,1,5). The measurement conditions are given in Table I.

tural model and the original diffraction data with the predictions and assumptions associated with a Landau-type description of the soliton regime is presented. Taking into account the experimental accuracy and the inevitable Fourier truncation effects, we will show that the experimental structural modulation agrees with this description. In particular, the simple theoretical relation between fifth-order and first-order satellite intensities, only dependent on the soliton density, is confirmed.

II. EXPERIMENT

The crystals were grown isothermally at 310 K by the dynamic method from acid aqueous solutions ($p\mathrm{H} \leqslant 2$) which contained a stoichiometric ratio of rubidium chloride and zinc chloride. The product of synthesis was purified by recrystalization from distilled water. The chemical composition of the crystal was confirmed by atomic spectrometry and chemical analysis. Crystals of the same synthesis product were also used for the investigation in Aramburu *et al.*,[25] where satellites of fifth-order were already reported. Figure 2 shows representative reflection profiles of a main reflection and several satellite reflections of each order. The average intensity relationship between main reflections, first-order satellites and fifth-order satellites is approximately $I_0 \approx 10I_1 \approx 700I_5$. The $\mathbf{q}$ vector describing the satellite reflections is given by $\mathbf{q}=\left[\frac{1}{3}-\delta(T)\right]\mathbf{c}^*$. At $T \rightarrow T_{\text{Lock-in}}$, $\delta(T) \rightarrow 0$ and $\mathbf{q} \rightarrow \mathbf{q_L}=\frac{1}{3}\mathbf{c}^*$, which implies that satellite reflections gradually superimpose, as the lock-in temperature is approached. To overcome the experimental difficulties associated with the detections of extremely weak and partially overlapped intensities of reflections, the use of synchrotron radiation was indispensable. Therefore, the measurement of diffraction intensities was carried out at the beamline F1 at the Hamburger Synchrotronstrahlungslabor (HASYLAB/DESY). Various crystals of high quality were preselected using laboratory equipment. The intensity measurements were realized on a kappa diffractometer equipped with a scintillation counter and a nitrogen cryostat from Oxford Cryosystems at a temperature of 194(1) K.

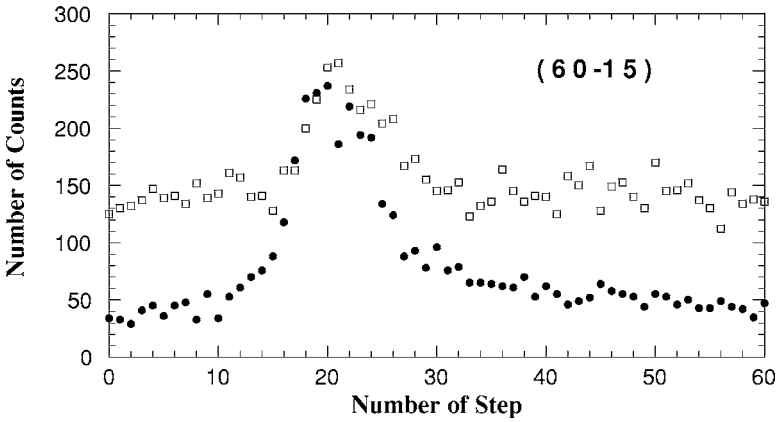

FIG. 3. Profile of the satellite reflection $(6,0,-1,5)$ measured at a wavelength of 0.7293 Å (empty squares) and 0.8265 Å (full dots). Measurement parameters are identical for both wavelengths.

The value of the **q** vector ($0.316\mathbf{c}^*$) was determined from the positions of selected satellite reflections. Our interest was centered on the intensities of satellite reflections of the fifth order (see above), which were expected to be extremely weak. Due to the limited time available at the synchrotron, we were not able to measure a complete dataset of satellites of the fifth order. Instead, we measured the intensities of selected reflections, for which, based on the predictions from theory,[25,27] we expected a relatively high signal. Preliminary studies of a comparatively small crystal of very good quality (as demonstrated by the extremely sharp reflection profiles of the main reflections) showed that satellite intensities of the fifth order were, unfortunately, extremely weak and even at the synchrotron source hardly detectable. We therefore decided to switch to a large crystal (with less ideal reflection profiles of the main reflections), this way achieving higher intensities which could be recorded more easily.

Initially, our idea was to measure at a wavelength similar to Mo K_α to keep the synchrotron dataset easily combinable to laboratory data. However, the bad peak to background ratio, which we attribute to fluorescence scattering implied by the neighborhood to the Rb-absorption edge, forced us to move to a wavelength more distant to this edge (0.8265 Å). Figure 3, which shows the profile of the same satellite reflection of the fifth order at the two wavelengths, demonstrates nicely that by switching the wavelength the peak to background ratio could be considerably improved. The choice of the wavelength suggested to measure also the main reflections and satellites of first order and second order, which was realized, within the limits of time (see Table I).

Satellites of third order are extremely close to the main reflections ($3\mathbf{q}=3\cdot 0.316\mathbf{c}^*=0.948\mathbf{c}^*$) and it is in general not possible to measure them reliably. Only where the main reflections are extinguished due to the extinction rules of the glide plane of the superspace group $Pmcn(00\gamma)ss$ it was possible to detect satellites of the third order as the extinction rules do not apply to them. The profiles of these satellites, however, show them to be extremely weak and far from ideal, so that their information content is limited. Several trials were undertaken to detect satellite reflections of the fourth order, yet, as we were not able to register any significant intensity, we discarded to measure at these positions.

For a numerical absorption correction the rather irregular crystal shape was approximated by 22 faces. The correction was carried out with the program JANA2000 (Ref. 28), which was modified for this purpose. The measurement conditions for the different types of reflections and the number of reflections recorded are given in Table I. Further experimental details are listed in Table II.

III. STRUCTURE SOLUTION

For structure refinement the program JANA2000 (Ref. 28) was used. As a starting model the parameters of the basic structure as given in Quilichini *et al.*[20] were entered. After the refinement of the structural parameters of the average structure taking into account the main reflections only, we subsequently refined the modulation amplitudes of the different harmonics, starting with the amplitudes of the harmonics of first order. Initially, we refined the amplitudes of the second harmonic and afterwards adjusted the amplitudes of the fifth harmonic. Yet this refinement strategy led to very bad

TABLE I. Measurement parameters and number of measured/independent reflections.

Satellite index	Number of steps	Time per step (s)	Measured reflections	Measured reflections $>3\sigma$	Independent reflections in refinement	Independent reflections $>3\sigma$ in refinement
0	61	0.4	1050	1050	784	778
1	61	0.4	676	666	473	473
2	61	2	438	340	271	251
3	61	4	386	80	55	53
5	81	4	354	241	156	140

TABLE II. Experimental details and crystallographic data of Rb_2ZnCl_4.

Crystal data	
Empirical formula	Rb_2ZnCl_4
Superspace group	$Pmcn(00\gamma)ss$
a, b, c (Å)	7.241(3), 12.648(5), 9.216(3)
q vector	0.316 $\mathbf{c}^*$
V (Å^3)	845.4
Z	4
D_x (Mg m^{-3})	6.206
Radiation type	Synchrotron (Hasylab, Hamburg, Germany)
No. of reflections for cell parameters	25
θ range (°)	2–31.4
μ (mm^{-1})	15.54
Temperature (K)	194(1)
Crystal form, color	Irregular, transparent
Crystal size (mm)	$0.13\times0.20\times0.33$
Data collection	
Diffractometer	Kappa-diffractometer (beamline F1)
Detector	Scintillation counter
Scan type	Ω
Absorption correction	Gaussian
Crystal approximated by	22 faces
T_{min}	3.18
T_{max}	35.34
No. of measured and observed reflections ($>3\sigma$)	2904, 2377
R_{int}	0.1276
θ_{max} (°)	31.4
Range of h,k,l,m	$0\rightarrow9,-10\rightarrow15,-9\rightarrow12,-5\rightarrow5$
Refinement	
Refinement on	F
GoF(all), GoF(obs)	9.15, 9.25
No. of reflections and parameters	1739 reflections ($1695>3\sigma$), 115 parameters
Weighting scheme	$w=1/[\sigma^2(F_0^2)]$
$(\Delta/\sigma)_{max}$	0.0001
$\Delta\rho_{max}$, $\Delta\rho_{min}$ (e Å^{-3})	2.37, −1.97

agreement factors for the satellites of the fifth order. We therefore reversed the order of refinement, refining the amplitudes of the fifth harmonic before the amplitudes of the second harmonic. This way we achieved clearly better agreement factors for the satellites of the fifth order, while the agreement factors for satellites of the second order stayed in a comparable range to the ones obtained in the first trial. The modulation amplitudes of the third harmonic were refined at the end. Attempts to refine the amplitudes of the fourth harmonics did not lead to values significantly different from zero and were therefore discarded.

As can be seen from Table III, the agreement factors for the main reflections are rather large. Therefore, we also tried to refine the atomic positions of the average structure on the basis of a disordered model as proposed by Itoh *et al.*,[29] yet this alternative model did also not yield better results. A possible explanation for these large agreement factors of the main reflections could be the very large size of the crystal, which was indispensable to obtain sufficient intensity for the weak satellite reflections. A consequence of this large size was that in certain positions the crystal was not fully bathed in the primary beam. This might imply systematic errors in the absorption correction and consequently have its effect on the overall agreement factors. This type of errors, somehow proportional to the peak intensity, is bound to be more significant for the main reflections, while for the weaker satellites intensity-independent errors associated with the experimental noise are much more important.

TABLE III. Final agreement factors for Rb_2ZnCl_4. $M=0$ corresponds to main reflections, and $M=1,2,3,5$ corresponds to satellites of the respective order.

Reflections	R(obs)	R_w(obs)	R(all)	R_w(all)
All	0.0836	0.1429	0.0844	0.1432
$M=0$	0.0810	0.1358	0.0814	0.1358
$M=1$	0.0714	0.0897	0.0714	0.0897
$M=2$	0.2100	0.2585	0.2250	0.2600
$M=3$	0.3771	0.4707	0.3988	0.4749
$M=5$	0.2205	0.2731	0.2254	0.2737

Possible modulation of the atomic displacement parameters (ADP) corresponding to modulation of the atomic thermal vibrations was not taken into account in the final model, as this would have increased the number of parameters dangerously, especially in view of the limited number of reflections available. Trial refinements, however, show that the introduction of these modulations have a considerable effect on the agreement factors for the satellite reflections (roughly a decrease of 0.02 for the first-order, 0.06 for the second-order, 0.08 for the third-order, and 0.05 for the fifth-order satellites).

It is important to stress that in this highly anharmonic structure, each Fourier term in the atomic modulations may have significant contributions not only to the satellites of the same order, but also to satellites of neighboring orders. Thus, for instance, Fourier terms of the third order are very important for refining the second-order satellites and the main information concerning these parameters originates from the second-order satellites. The very few third-order satellites, which we were able to measure, are very badly adjusted by our model and do not seem to contain any significant information about the Fourier terms of the third order. Due to the small number of observations (see Table I), the weight of these reflections in the refinement is very small. In addition, their profile shapes are far from being ideal, making it difficult to extract their intensities reliably. Even when introducing more parameters (modulation of ADPs, refinement of Fourier terms of the fourth order), we were not able to adjust these intensities in a more satisfactory way.

The atomic coordinates, ADP parameters, and amplitudes of the modulation function of the final model are given in Tables IV–VI. Further details of the crystallographic investigations can be obtained from the Fachinformationszentrum Karlsruhe, D-76344 Eggenstein-Leopoldshafen, Germany, on quoting the depository number CSD 415861.

TABLE IV. Atomic coordinates and isotropic displacement parameters of Rb_2ZnCl_4.

Site	x	y	z	U_{iso}
Rb1	0.25	0.406 18(20)	0.6299(2)	0.0499(8)
Rb2	0.25	0.819 38(12)	0.486 83(19)	0.0307(6)
Zn	0.25	0.421 84(12)	0.223 07(18)	0.0236(6)
Cl1	0.25	0.4195(3)	−0.0179(4)	0.0445(14)
Cl2	0.25	0.5845(3)	0.3216(5)	0.0427(13)
Cl3	0.0026(4)	0.3388(3)	0.3108(4)	0.0467(10)

IV. COMPARISON WITH THE SOLITON MODEL

According to Table VI, the ratio among the amplitudes of the different harmonics of the structural modulation is

$$A_1 \approx 5.5A_3 \approx 10.5A_5 \approx 25.3A_2,$$

where A_n represents the average value of the amplitude moduli of the nth—order harmonic. The relative large strength of the fifth-order harmonic can be observed. In fact, the main contribution of the third-order harmonic is in the atomic modulations corresponding to Cl2(x) and Cl3(y). If these atomic modulations are not considered in the averaging process then $A_5 \approx A_3$.

According to the soliton model restricted to the so-called constant amplitude approximation,[5] the atomic modulations resulting from the existence of the order parameter modulation can be expressed as[30]

$$u_\alpha^\mu(v) = \rho e_\alpha^\mu \cos[2\pi\theta(v) + \varphi_\alpha^\mu], \tag{1}$$

where $\alpha=\{x,y,z\}$, μ labels the atoms in the unit cell, and $\{e_\alpha^\mu, \varphi_\alpha^\mu\}$ are the atomic amplitudes and phases corresponding to the eigenvector of the unstable mode. The variable v represents the internal coordinate in the $(3+1)$ superspace description,[31] so that the atomic displacements realized at an average unit cell $\mathbf{l}$ are given by $u_\alpha^\mu(v=\mathbf{q}\cdot\mathbf{l})$ ρ is the constant amplitude of the order parameter, while its modulated phase $2\pi\theta(v)$ satisfies the sine-Gordon equation[30]

TABLE V. Anisotropic displacement parameters of Rb_2ZnCl_4.

Site	$u11$	$u22$	$u33$	$u12$	$u13$	$u23$
Rb1	0.0496(14)	0.0740(17)	0.0249(11)	0	0	−0.0028(9)
Rb2	0.0398(11)	0.0253(11)	0.0272(12)	0	0	−0.0003(6)
Zn	0.0230(10)	0.0241(10)	0.0238(10)	0	0	0.0007(6)
Cl1	0.074(3)	0.039(2)	0.020(2)	0	0	−0.0054(15)
Cl2	0.069(3)	0.031(2)	0.027(2)	0	0	−0.0053(16)
Cl3	0.0307(15)	0.064(2)	0.0458(16)	−0.0186(15)	−0.0020(13)	0.0135(17)

TABLE VI. Modulation amplitudes (multiplied by 10^4) of Rb_2ZnCl_4.

Site	Order of harmonics	x sin	y sin	z sin	x cos	y cos	z cos
Rb1	1	126(4)	0	0	−120(4)	0	0
	2	0	−4(2)	11(2)	0	−23(2)	4(2)
	3	−10(4)	0	0	−1(4)	0	0
	5	14(2)	0	0	−15(2)	0	0
Rb2	1	172(3)	0	0	−11(3)	0	0
	2	0	1.5(11)	−7(2)	0	1.1(11)	0(2)
	3	−11(4)	0	0	−12(4)	0	0
	5	12(2)	0	0	2(2)	0	0
Zn	1	104(3)	0	0	33(3)	0	0
	2	0	−3.9(12)	0(2)	0	0.3(12)	4(2)
	3	1(3)	0	0	−18(3)	0	0
	5	−11(2)	0	0	−1(2)	0	0
Cl1	1	401(9)	0	0	72(8)	0	0
	2	0	−10(4)	−3(5)	0	−14(4)	−1(5)
	3	8(9)	0	0	15(8)	0	0
	5	39(5)	0	0	0(7)	0	0
Cl2	1	83(9)	0	0	545(9)	0	0
	2	0	−2(5)	4(5)	0	−8(3)	14(5)
	3	−73(11)	0	0	−131(10)	0	0
	5	26(7)	0	0	27(8)	0	0
Cl3	1	59(5)	−6(3)	−114(4)	−187(5)	271(3)	146(5)
	2	6(5)	−2(4)	3(4)	5(4)	−5(3)	7(4)
	3	−16(5)	15(3)	23(6)	27(5)	−72(3)	−32(7)
	5	−27(4)	17(4)	21(3)	0(3)	16(4)	3(3)

$$\left[\frac{d\theta(v)}{dv}\right]^2 = \frac{1}{n_s^2}\{1 - k^2 \sin^2[6\pi\theta(v)]\}, \tag{2}$$

where k is related with the soliton density n_s through the relation $n_s = \pi/[2K(k)]$, $K(k)$ being the complete elliptic integral of the first kind. The approximate steps of the order parameter phase $2\pi\theta(v)$ occur at values $\pi/2 + n\pi/3$ ($n = 0, 1\ldots$) (see Fig. 1), which correspond to the six possible phase values of the order parameter in the lock-in phase, each value being associated to one of the six possible domains in this phase. It is important to note that although the width of the discommensurations of $\theta(v)$ in the internal space goes to zero when the narrow-soliton regime is approached ($n_s \to 0$), in the usual Landau description in real space the width of the discommensurations of $\theta(z)$ is preserved finite by the simultaneous blow-up of the scale factor δ^{-1} that relate both descriptions ($z = \delta^{-1}v$; $\delta \equiv |\mathbf{q} - \mathbf{q_L}|$) when the lock-in limit is approached.[30]

Equation (1) represents very strong restrictions on the possible forms of the Fourier series describing the atomic modulation functions $u_\alpha^\mu(v)$. We can now examine the degree of fulfillment of these restrictions in the refined structural model reported in the previous section.

Using some general properties[30] satisfied by the function $\theta(v)$, namely $\theta(-v) = -\theta(v)$ and $\theta(v + \frac{1}{6}) = \theta(v) + \frac{1}{6}$, it can be demonstrated that

$$\Delta\theta(v) \equiv \theta(v) - v = \sum_{n=1}^{\infty} c_n \sin(2\pi 6nv) \tag{3}$$

and

$$\cos[2\pi\theta(v)] = \sum_{\{m_p\}} \left[\prod_{p=1}^{\infty} J_{m_p}(2\pi c_p)\right] \times \cos\left[2\pi\left(1 + 6\sum_{p=1}^{\infty} \mathrm{p.m}_p\right)v\right] \equiv a_1 \cos(2\pi v) + \sum_{j=1}^{\infty} a_{6j\pm1} \cos[2\pi(6j \pm 1)v], \tag{4}$$

$$\sin[2\pi\theta(v)] = \sum_{\{m_p\}} \left[\prod_{p=1}^{\infty} J_{m_p}(2\pi c_p)\right] \times \sin\left[2\pi\left(1 + 6\sum_{p=1}^{\infty} \mathrm{p.m}_p\right)v\right] \equiv b_1 \sin(2\pi v) + \sum_{j=1}^{\infty} b_{6j\pm1} \sin[2\pi(6j \pm 1)v], \tag{5}$$

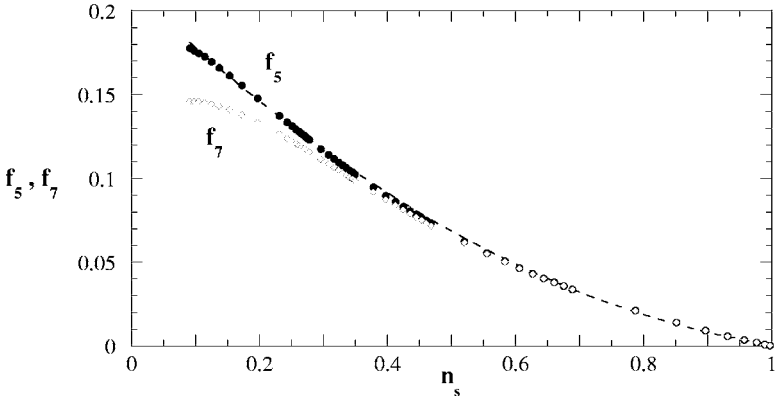

FIG. 4. Functions $f_5(n_s)$ (full dots) and $f_7(n_s)$ (empty rhombs) giving the ratio of the amplitudes of the fifth-order and seventh-order harmonics, respectively, with respect to the first-order harmonic of the structural modulation, as a function of the soliton density, according to the soliton model with six steps. The inverse function for $f_5(n_s)$ can be approximated by $n_s=1.19-\sqrt{0.03+6.5(|a_5|/|a_1|)}$ (discontinuous line).

where the first sum in (4) and (5) is extended to all possible sets $\{m_p\}$ of integer indices of the Bessel functions. Thus, only harmonics of orders $n=\{1,6j\pm1\}(j\in Z^+)$ are present in the Fourier expansion of $\{\cos[2\pi\theta(v)],\sin[2\pi\theta(v)]\}$. In addition, the coefficients of both expansions are related as follows:

$$\begin{cases} b_n = a_n & \text{if } n = 1,\ 6j+1 \\ b_n = -a_n & \text{if } n = 6j-1. \end{cases} \tag{6}$$

The specific value of the coefficients a_n will depend on the shape of the function $\theta(v)$, which is controlled by the soliton density n_s [Eq. (2)]. Using Eqs. (4)–(6), the expression (1) for the atomic modulation functions $u_\alpha^\mu(v)$ can be transformed into a Fourier series

$$u_\alpha^\mu(v) = \sum_{j=0}^{\infty} u_{6j+1,\alpha}^\mu \cos[2\pi(6j+1)v + \varphi_\alpha^\mu] + \sum_{j=1}^{\infty} u_{6j-1,\alpha}^\mu \cos[2\pi(6j-1)v - \varphi_\alpha^\mu + \pi] \tag{7}$$

with the amplitudes given by

$$u_{6j\pm1,\alpha}^\mu = (\rho e_\alpha^\mu)|a_{6j\pm1}| \tag{8}$$

Hence, the soliton configuration of the order parameter only produces atomic Fourier terms of order 1,5,7,11,13,… in the atomic modulation functions. Their amplitude ratios are independent of the atom μ and component α, and depend only on the order of the term and the soliton density

$$\frac{u_{6j\pm1,\alpha}^\mu}{u_{1,\alpha}^\mu} = \frac{|a_{6j\pm1}|}{|a_1|} \equiv f_{6j\pm1}(n_s) \tag{9}$$

The functions $f_{6j\pm1}(n_s)$, that depend only on the soliton density, have the values $1/(6j\pm1)$ as limit in the ideal steplike case corresponding to $n_s=0$.

In order to compare the phases of the Fourier terms given in Eq. (7) with the phases $\{\Psi_{n,\alpha}^\mu\}$ of the modulation functions determined in the structural refinement, a change of variable is required. The atomic modulation functions of incommensurate structures are conventionally described with respect to the internal variable $x_4^\mu \equiv \mathbf{q}\cdot(\mathbf{l}+\mathbf{r}_{\rm av}^\mu) \approx v + \mathbf{q_L}\cdot\mathbf{r}_{\rm av}^\mu$, where $\mathbf{r}_{\rm av}^\mu$ is the average position of atom μ in the unit cell. Eq. (7) becomes then

$$u_\alpha^\mu(x_4^\mu) = \sum_{j=0}^{\infty} u_{6j+1,\alpha}^\mu \cos[2\pi(6j+1)x_4^\mu + \Psi_{6j+1,\alpha}^\mu] + \sum_{j=1}^{\infty} u_{6j-1,\alpha}^\mu \cos[2\pi(6j-1)x_4^\mu + \Psi_{6j-1,\alpha}^\mu] \tag{10}$$

with all the phases directly related with the one of the first harmonic ($\Psi_{1,\alpha}^\mu = \varphi_\alpha^\mu - 2\pi\mathbf{q_L}\cdot\mathbf{r}_{\rm av}^\mu$) in the form

$$\Psi_{6j+1,\alpha}^\mu = \Psi_{1,\alpha}^\mu - 2\pi(6j)\mathbf{q_L}\cdot\mathbf{r}_{\rm av}^\mu, \tag{11}$$

$$\Psi_{6j-1,\alpha}^\mu = -\Psi_{1,\alpha}^\mu - 2\pi(6j)\mathbf{q_L}\cdot\mathbf{r}_{\rm av}^\mu + \pi. \tag{12}$$

Hence, the soliton model implies a very specific relation between the amplitudes and phases of the first and fifth harmonic of the modulation functions

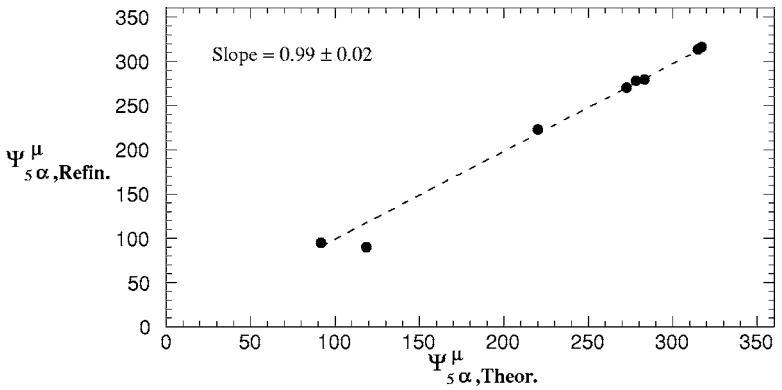

FIG. 5. Comparison of the phases (in degrees) corresponding to the fifth-order harmonic obtained in the refinement: $\Psi_{5\alpha,\text{Refin.}}^\mu$ ($\mu=\{1,\ldots,s\}$; $\alpha=\{x,y,z\}$), with the theoretical values of the phases according to the soliton model deduced from Eq. (14): $\Psi_{5\alpha,\text{Theor.}}^\mu = -\Psi_{1\alpha,\text{Refin.}}^\mu - 360(z_{\text{ave,Refin.}}^\mu) + 180$.

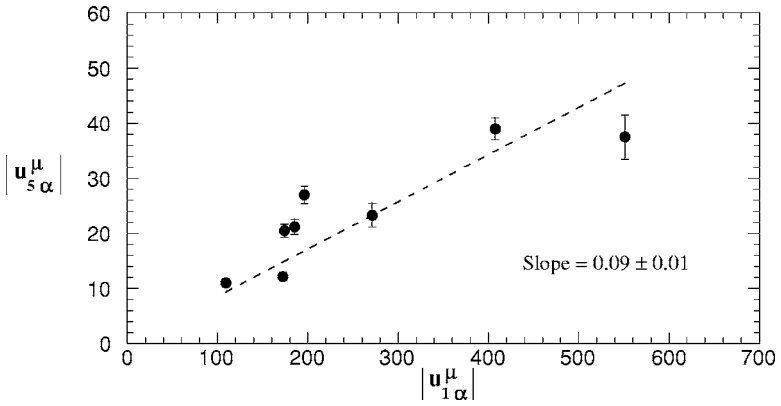

FIG. 6. Comparison of the amplitudes (multiplied by 10^4) corresponding to the first-order harmonic and the fifth-order harmonic obtained in the refinement for all independent atoms $\mu=\{1,\ldots,s\}$ and spatial directions $\alpha=\{x,y,z\}$. The amplitudes are in cell units. The slope of the straight line obtained in a linear fitting to the points is 0.09±0.01.

$$\frac{u^{\mu}_{5,\alpha}}{u^{\mu}_{1,\alpha}} = f_5(n_s) \quad \forall\{\alpha,\mu\}, \tag{13}$$

$$\Psi^{\mu}_{5,\alpha} = -\Psi^{\mu}_{1,\alpha} - 4\pi z^{\mu}_{\mathrm{av}} + \pi. \tag{14}$$

The function $f_5(n_s)$ is shown in Fig. 4. In Fig. 5 the phases of the fifth-order harmonic obtained in the refinement $\{\Psi^{\mu}_{5,\alpha\ \mathrm{Refined}}\}$ are compared with those deduced, using Eq. (14), from the values of $\{\Psi^{\mu}_{1,\alpha\ \mathrm{Refined}}, z^{\mu}_{\mathrm{ave.\ Refined}}\}$ obtained in the refinement for $\alpha=\{x,y,z\}$ and $\mu=\{1,\ldots,s\}$. It is evident that the correlations expressed by Eq. (14) are very well satisfied. It must be stressed that the refinement did not include any a priori restriction on these phase values. The correlation between the corresponding refined amplitudes of the first-order and fifth-order harmonics is shown in Fig. 6. Although worse than for the phases, an approximate global linear correlation can be observed. A linear fitting to the experimental points yields a slope of 0.09±0.01, which can be identified with the approximate value of $f_5(n_s)$.

It is important to note that the soliton model and the resulting strong correlations between the first and fifth harmonics can be cross-checked by analyzing directly the experimental diffraction diagram. It can be demonstrated[27] that in a soliton configuration as the one described above the quotient between the structure factor of a first-order satellite $\mathbf{H}=(\mathbf{G},h_4=\pm1)$ and that of the closest fifth-order satellite $\mathbf{H}'=(\mathbf{G}',h_4=\pm5)$, so that $\mathbf{G}\pm\mathbf{q_L}=\mathbf{G}'\pm5\mathbf{q_L}$ (where $\mathbf{G},\mathbf{G}'$ are vectors of the reciprocal lattice of the average structure), is approximately the same for all such pairs of reflections

$$\frac{|F(\mathbf{G}',h_4=\pm5)|}{|F(\mathbf{G},h_4=\pm1)|} \approx \frac{\left|\int_0^1 \cos\{2\pi[\theta(v)+5v]\}dv\right|}{\left|\int_0^1 \cos\{2\pi[\theta(v)-v]\}dv\right|} \quad \forall\,\mathbf{G}. \tag{15}$$

This ratio only depends on the function $\theta(v)$ and, therefore, on the soliton density. In fact, according to Eqs. (4)–(6)

$$\int_0^1 \cos\{2\pi[\theta(v)+5v]\}dv = a_5, \tag{16}$$

$$\int_0^1 \cos\{2\pi[\theta(v)-v]\}dv = a_1, \tag{17}$$

and using Eq. (9) we finally obtain

$$\frac{|F(\mathbf{G}',h_4=\pm5)|}{|F(\mathbf{G},h_4=\pm1)|} \approx \frac{u^{\mu}_{5,\alpha}}{u^{\mu}_{1,\alpha}} = \frac{|a_5|}{|a_1|} = f_5(n_s). \tag{18}$$

Therefore, according to the soliton model, the quotient between the moduli of the structure factors of pairs of close first-order and fifth-order satellites should be constant. From this number the soliton density corresponding to the structural modulation can be determined through the function $f_5(n_s)$ (see Fig. 4). This important property was already pointed out in Ref. 27 Here we have shown in addition that this quotient approximately equals the quotient between the amplitudes of first-order and fifth-order harmonics which, as

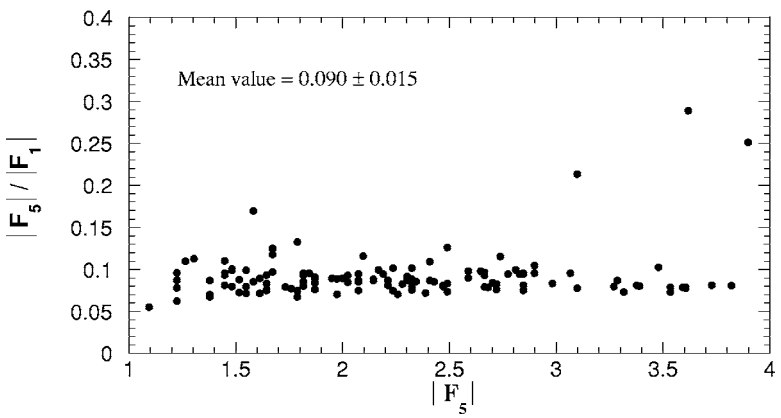

FIG. 7. Set of ratios between the experimental structure factors of the observed fifth-order and first-order satellites. Every observed fifth-order satellite has been paired with the first-order satellite closest in the diffraction pattern. It can be observed that the ratio is approximately the same for all pairs, in agreement with the soliton model prediction. The average value obtained from a statistical analysis of the distribution of ratios is: 0.090±0.015, the same value as the one determined from the ratio of the amplitudes of the first-order and the fifth-order harmonics in Fig. 6.

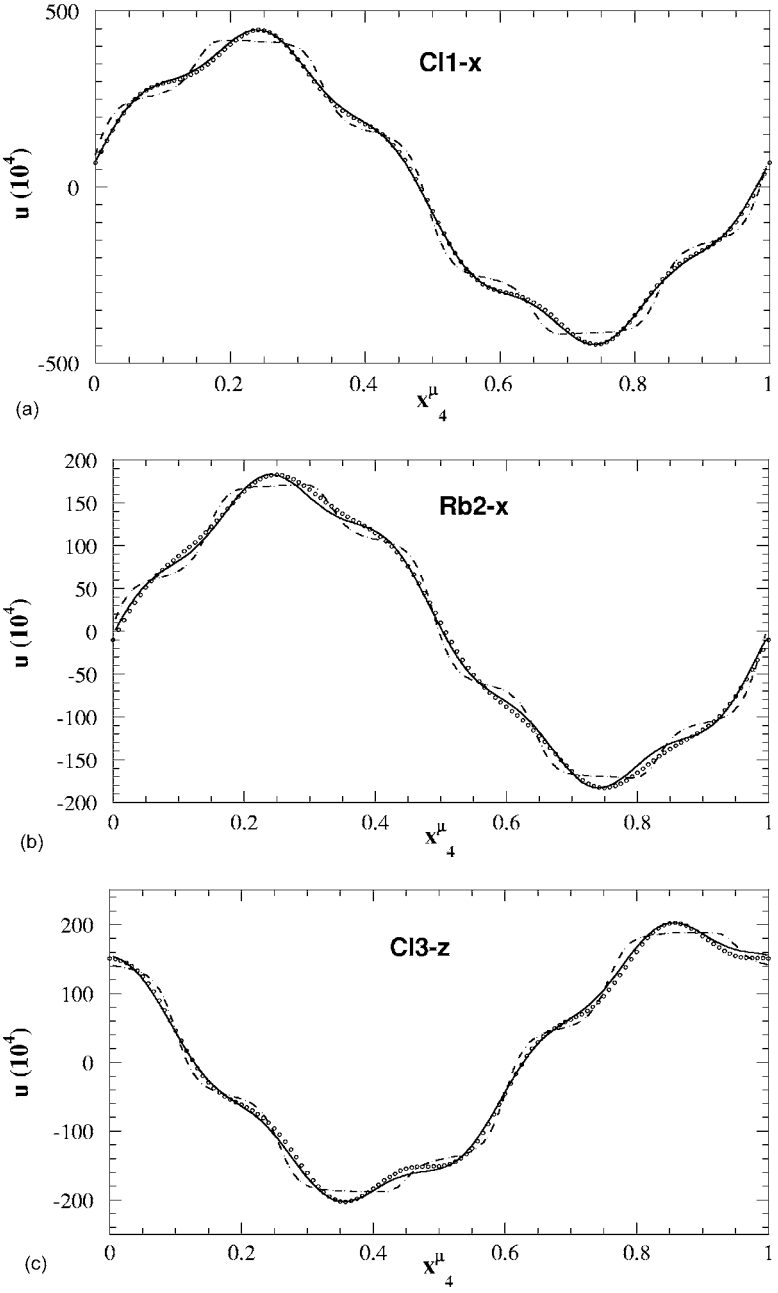

FIG. 8. Comparison between the experimental modulation corresponding only to the first-order and fifth-order harmonics obtained in the refinement (empty dots), and the atomic modulations obtained from the soliton model with $n_s=0.4$ considering only the first-order and fifth-order harmonics (continuous line) and all harmonics (broken line) for: (a) Cl1-*x*, (b) Rb2-*x*, and (c) Cl3-*z*. The difference between the continuous line and the broken line is practically due to the seventh-order harmonic. It can be observed that, when only the first-order and fifth-order harmonics are considered, the agreement between the experimental and the theoretical atomic modulations is very good.

discussed above, is also a constant, independent of atom and coordinate. Although particularized above for fifth-order satellites, an analogous relation exists for satellites of any order of type $6j\pm1$.

In Fig. 7 the set of ratios between the experimental structure factors of the observed first-order and fifth-order satellites is shown. As predicted by the soliton model, the quotient is approximately the same for all pair of reflections giving a value $|F(\mathbf{G}',h_4=\pm5)|/|F(\mathbf{G},h_4=\pm1)|=0.090\pm0.015$. This value coincides with the one obtained from the linear fit of the harmonic amplitudes in Fig. 6. According to Fig. 4 and Eq. (18), it corresponds to a soliton density $n_s\approx0.4\pm0.05$. This soliton density agrees within experimental accuracy with the ones determined by nuclear magnetic resonance (NMR) (Ref. 10) ($n_s\approx0.45$) and dielectric measurements[18] ($n_s\approx0.35$) at the same temperature.

It can be concluded that the diffraction data and the resulting structural model are in very good agreement with the predictions obtained from the soliton model. First-order and fifth-order harmonics of the modulation satisfy approximately a very simple correlation which indicates a soliton density of the order of 0.4. Second-order, third-order, and fourth-order Fourier terms are irrelevant for the primary distortion associated to the order parameter and its modulation. In fact, the detected second and third harmonics of the atomic modulations correspond to secondary modes, of different symmetry, that also become frozen in the incommensurate phase. They will be analyzed in the next section.

The observation of the soliton configuration in the atomic modulations, as ideally represented in Fig. 1, is hampered by the unavoidable truncation of the experimental modulations. From the analysis above it seems clear that the actual struc-

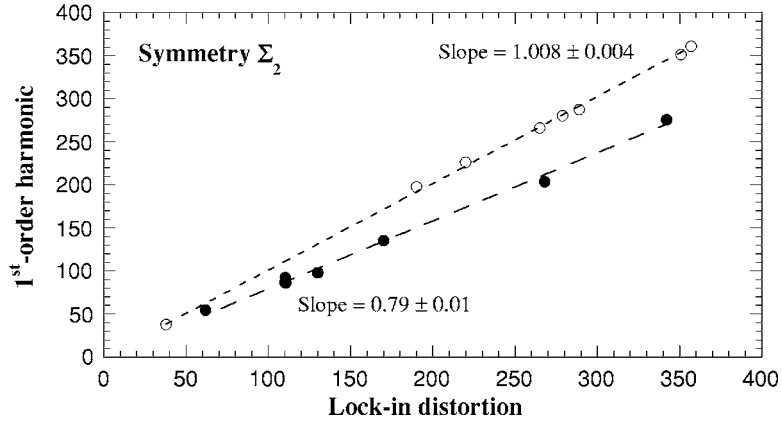

FIG. 9. Comparison of the amplitudes (black points) and phases (empty dots) corresponding to the first-order harmonic obtained in the refinement and the lock-in distortion of symmetry Σ_2 at 100 K for all independent atoms $\mu=\{1,\ldots,s\}$ and spatial directions $\alpha=\{x,y,z\}$. The amplitudes and phases of the Σ_2 distortion in the lock-in phase have been taken from the Table III of Ref. 25. The amplitudes are in cell units of the average structure multiplied by a factor 10^4, and the phases are in degrees. The amplitudes of the first-order harmonic have been divided by 2 in order to make them comparable with the moduli of the complex amplitudes of the lock-in distortion that appear in Ref. 25. A phase of 180° has been added to the phases of the lock-in distortion due to the opposite twin choice in the description of the two structures compared.

tural modulation must also have a significant contribution of terms higher than the fifth one. These higher-order Fourier terms, close to or beyond the experimental resolution are important for obtaining atomic modulations functions consistent with the soliton description. In Fig. 8 some of the experimental refined modulations restricted to the first-order and fifth-order harmonics (empty dots), are compared with the theoretical atomic modulations obtained from the soliton model with $n_s=0.4$ considering only the first-order and fifth-order harmonics (continuous line) and all harmonics (broken line). It can be clearly seen, that the functions obtained truncating the ideal series associated with the soliton model agree very well with the experimental modulations, and it becomes evident that the experimental truncation up to fifth order of the atomic modulations strongly blurs the existing steps corresponding to the quasicommensurate regions.

The most important missing term in the experimental modulation is the seventh-order one. Some satellites of this order were indeed detected by Andrews *et al.*[24] and Aramburu *et al.*[25] but their intensities were much weaker than those of the fifth order, typically a factor of the order of 3. Because of this reason and due to the limited measurement time available at the synchrotron source the measurement of seventh-order satellites was discarded *a priori*. The limits of $f_5(n_s)$ and $f_7(n_s)$ for $n_s=0$, i.e., at the ideal limit of the soliton modulations, are 1/5 and 1/7, respectively (see Fig. 4). This means that in fact, in the idealized steplike limit, seventh-order satellites would be about half as weak as their neighboring satellites of the fifth order. However, according to Eq. (9) and Fig. 4, in an intermediate soliton regime with a soliton density of 0.4, as the one estimated above, the amplitudes of the seventh-order harmonics should be much closer to those of the fifth order. This means that in general seventh-order satellites would have intensities weaker but similar to those of the fifth order. This contrasts with the few experimental observations of the seventh-order satellites mentioned above[24,25] which suggest that the seventh-order satellites are systematically much weaker than their neighboring fifth-order ones. The reason for this apparent discrepancy of the behavior of the seventh-order satellites with respect to the predictions of the soliton model is unclear, especially considering the extreme success of the soliton model in explaining the diffraction diagram up to the fifth-order satellites, as shown above. The reason is probably the systematic degradation of the quality of the satellites with their order. Small inhomogeneities in the sample are bound to produce a certain distribution of wave vector values that results in an intrinsic width of the satellites which increases linearly with the satellite order. In any case, systematic measurements of the seventh-order satellites would be required to assess the situation with respect to the contribution of harmonics of this order to the atomic modulations.

V. MODE EIGENVECTORS AND COMPARISON WITH THE LOCK-IN PHASE

The complex amplitudes of a given harmonic n corresponding to the modulations of atoms related by the superspace group operations can be written in the form of a symmetry mode. It can be shown[32] that, if the symmetry mode is expressed in terms of the wave vector $(\mathbf{q}'+n\boldsymbol{\delta})$, where $\boldsymbol{\delta}=\delta(T)\mathbf{c}^*$, $n\mathbf{q_L}=\mathbf{G}+\mathbf{q}'$ with $\mathbf{q}'\in\{\mathbf{q_L},-\mathbf{q_L},\mathbf{0}\}$, the harmonics of order $n=0$, $6m$ $(m\neq 0)$, $6m\pm 1$, $6m\pm 2$, $6m+3$ $(m\in Z)$ have symmetries A_{1g}, Σ_1, Σ_2 (antisymmetric for C_{2x} and C_{2y}), Σ_4 (antisymmetric for C_{2y} and C_{2z}) and Σ_3, respectively. The first-order, fifth-order, and all harmonics of order $6m\pm 1$ have symmetry Σ_2 and for $\boldsymbol{\delta}=\mathbf{0}$ they produce the reduction of symmetry to the space group $P2_1cn$ of the ferroelectric phase with a triplicated cell along $\mathbf{c}^*$. In this sense the distortion corresponding to these harmonics can be considered the primary mode, as discussed in the previous section. From this viewpoint, the very restrictive equations relating these terms, discussed above, can be considered equivalent to the assumption that the mode eigenvectors for

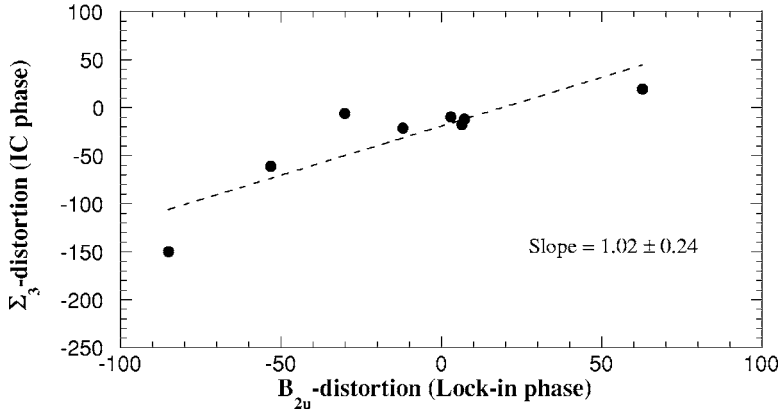

FIG. 10. Comparison between the distortion corresponding to the third-order harmonic obtained in the refinement (symmetry Σ_3) evaluated at $\mathbf{q}\equiv\mathbf{q_L}$ $[u^{\mu}_{3,\alpha}\cos(2\pi z^{\mu}+\Psi^{\mu}_{3,\alpha}+3\pi/2)]$, and the lock-in distortion of symmetry B_{2u} at 100 K for all independent atoms $\mu=\{1,\ldots s\}$ and spatial directions $\alpha=\{x,y,z\}$. The amplitudes of the B_{2u} distortion in the lock-in phase have been taken from Table II of Ref. 25. The amplitudes have been multiplied by (-1) in order to make them comparable with the distortion corresponding to the third-order harmonic, as both structures correspond to opposite twins. The displacements are in cell units of the average structure multiplied by a factor 10^4.

all relevant harmonic modes of symmetry Σ_2 superimposing in the structural distortion have the same eigenvector although their wave vectors $(6m\pm1)\mathbf{q}$ are different when reduced to the Brillouin zone. Thus, the displacement of a specific atom in the structure due to the Σ_2 order parameter distortion can be written as

$$\mathbf{u}^{\mu}_{\Sigma_2}(\mathbf{l}) = \Bigg(f_1(n_s) Q \mathbf{e}^{\mu}_{\Sigma_2} \exp[i(\mathbf{q_L}+\boldsymbol{\delta})\cdot\mathbf{r}^{\mu}(\mathbf{l})] + \sum_{j=1}^{\infty} \pm f_{6j\pm1}(n_s) Q \mathbf{e}^{\mu}_{\Sigma_2} \exp\{i[\pm\mathbf{q_L} + (6j\pm1)\boldsymbol{\delta}]\cdot\mathbf{r}^{\mu}(\mathbf{l})\} \Bigg) + \text{c.c.}, \tag{19}$$

where the sum includes both the terms indicated with plus and with minus sign, $\mathbf{e}^{\mu}_{\Sigma_2}$ is the complex eigenvector associated to the unstable mode, which is considered common for all harmonics 5, 7, 11, 13, etc… . Q is the complex mode amplitude of the first harmonic, which has an arbitrary phase in the incommensurate phase, while the functions $f_{6j\pm1}(n_s)$ are those defined in Eq. (9) [note that trivially $f_1(n_s)=1$]. $\mathbf{r}^{\mu}(\mathbf{l})$ is the position of the atom μ in the cell $\mathbf{l}$ of the basic nondistorted structure. In Eq. (19), the wave vectors[33] of the superimposing modes form a grid of vectors separated by 6δ along the $\mathbf{c}^*$ axis, centered around the incommensurate wave vector $\mathbf{q}$ of the first harmonic. This grid only collapses into a single wave vector $\mathbf{q_L}$ in the lock-in phase where $\boldsymbol{\delta}$ becomes zero. The assumption, based on the smallness of $\boldsymbol{\delta}$, of a common eigenvector for all superposing modes in (19), despite their wave vectors being different, is an essential point of the structural description which is implicit in the continuous approximation done when a generalized Landau-Ginzburg approach is applied. As shown in the previous section, this assumption is rather well satisfied, justifying the soundness of the Landau approach for describing the soliton regime of this type of compounds.

The second-order, third-order, and fourth-order harmonics correspond to secondary modes that give rise for $\boldsymbol{\delta}=\mathbf{0}$ to invariance groups of higher symmetry than $P2_1cn$. Hence, the amplitude of these harmonics are in principle expected to be small. The results obtained in the refinement indicate that the previous assessment is true for the second-order and the fourth-order harmonic, but not for the third-order one (see Table VI), which has significant amplitudes. The distortion corresponding to the third-order harmonic gives rise, for $\boldsymbol{\delta}=\mathbf{0}$, to the macroscopic polarization in the ferroelectric phase. Although, in contrast with assumptions done in earlier studies of this type of materials[34] this third harmonic associated with a long wavelength polarization wave is known at present not to be essential in the mechanism of the phase transitions sequence,[35] the present result indicates that at least this third-order modulation may play a significant role in the approach of the system to the lock-in transition. This contrasts with results recently reported for ammonium tetrafluoroberyllate, also a compound of type A_2BX_4 having a lock-in phase with duplication of the unit cell. In this compound the polarization wave could not be detected in the incommensurate phase.[36] Given the poor quality of the third-order satellites and their large R factors, commented in Sec. III, it may sound illusory to give much reality to the refined third-order harmonics of the atomic modulations. However, the soundness and validity of this harmonic can be cross-checked by comparison with the frozen polarization mode observed in the lock-in phase, as discussed below.

The lock-in phase can also be described as a distortion of the basic structure. This commensurate distortion can be decomposed in terms of symmetry modes of the basic structure according with the procedures shown in Ref. 37 or Ref. 38. In the case of Rb_2ZnCl_4, the contribution of each symmetry mode to the lock-in distortion is listed in Table II of Ref. 25 where the structural data at 300 K (basic structure) and 100 K (lock-in phase) have been taken from Quilichini and Pannetier.[20] Once this decomposition of the lock-in distortion

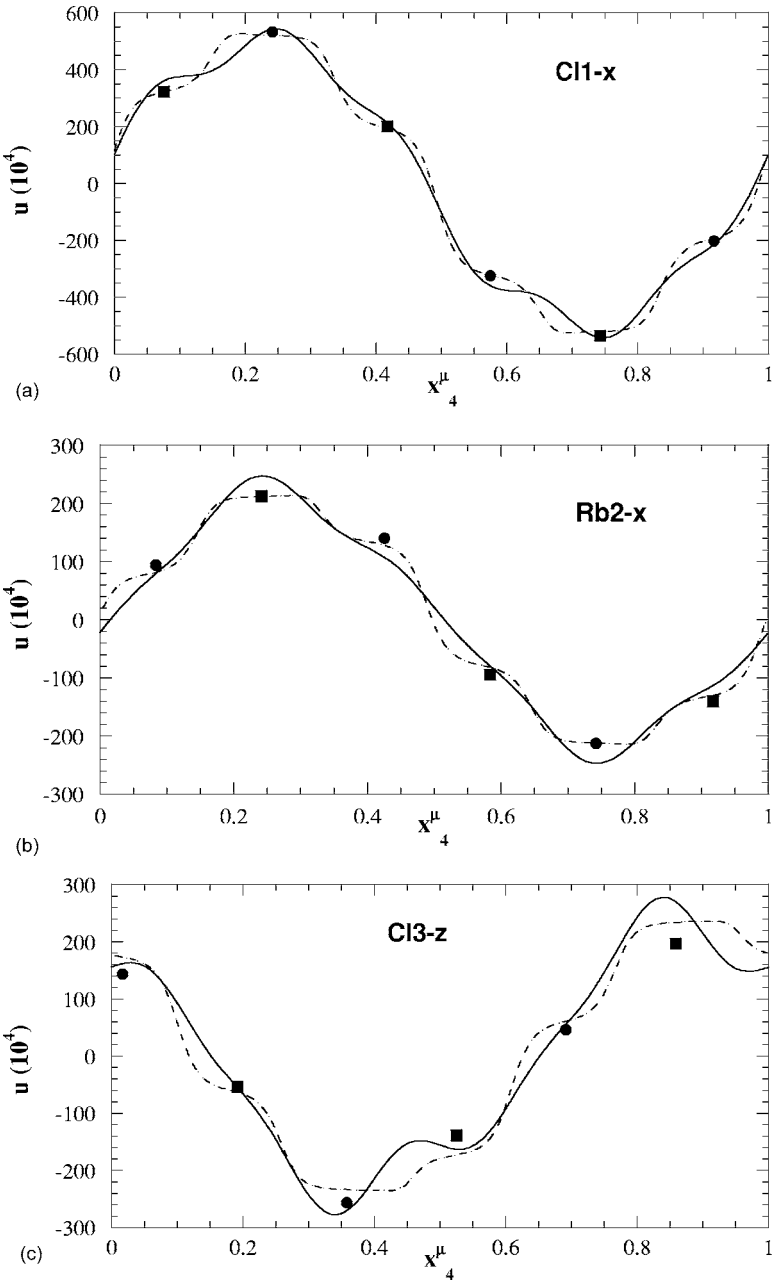

FIG. 11. Comparison between the structural modulation in the incommensurate phase obtained in the refinement and the atomic displacements in the lock-in phase, for: (a) Cl1-x, (b) Rb2-x, and (c) Cl3-z. The continuous line represents the atomic modulation function of the atom obtained multiplying the first-order and fifth-order harmonics of symmetry Σ_2 by $(0.79)^{-1} \cong 1.27$ and the third order harmonic of symmetry Σ_3 by 1. The dots and the squares represent the displacements of the independent atoms in the lock-in phase at 100 K respect to their positions in the basic structure. The dots correspond to the displacements of the atoms of three consecutive cells of the basic structure forming the triplicated unit cell of the lock-in phase. The squares represent the displacements of the atoms that in the incommensurate phase were related with the previous ones by the inversion center that is lost in the lock-in transition. The discontinuous line represents the total distortion of Σ_2 symmetry obtained from the soliton model with a soliton density $n_s=0.4$.

has been carried out, we can compare its component of a certain symmetry with the distortion (harmonic) of the same symmetry in the incommensurate phase. Thus, the first-order harmonic of the incommensurate distortion should be compared with the lock-in component of symmetry Σ_2. This is done in Fig. 9. It can be observed that the atomic amplitudes of both distortions are practically the same except for a global factor (slope=0.79) while the phases are equal (slope =1.008) except for a phase π due to the opposite twin election in the description of the two structures compared. This means that the eigenvector $\mathbf{e}^{\mu}_{\Sigma_2}$ observed in the incommensurate phase [see Eq. (19)] coincides with the one associated to the primary distortion in the lock-in phase.

The symmetry Σ_3 of the third-order harmonic becomes $B_{2u}(\mathbf{q}'=\mathbf{0})$ when $\mathbf{q}$ locks into $\mathbf{q_L}$, so that the distortion of the third-order harmonic should be compared with the lock-in distortion of symmetry B_{2u} (related with the macroscopic polarization in the ferroelectric phase). This comparison is shown in Fig. 10. It can be observed that both distortions are approximately the same (slope=1.02 ± 0.2), confirming the consistency and order of magnitude of the third-order harmonic obtained in the refinement. However, a much larger dispersion of the points than for the first harmonic is observed. This is consistent with the expected much larger experimental relative errors. Similar results are obtained when the amplitudes and phases of the second harmonic are compared with the lock-in distortion of symmetry Σ_4.

All these results show that the incommensurate distortion corresponding to every symmetry mode maintains its displacement pattern practically unaltered in the lock-in transition except for a global change in the amplitudes, and the change of wave vector into $\mathbf{q_L}$. In consequence, if the harmonics obtained in the refinement are multiplied by the cor-

responding global scale factors determined in the previous fittings, the global distortion thus obtained should describe in a very good approximation the atomic positions in the lock-in phase at 100 K. In Figs. 11(a)–11(c) both distortions are compared for Cl1-x, Rb2-x, and Cl3-z. The continuous line represents the atomic modulation function of the atom obtained multiplying each harmonic of Table VI by the mentioned fitted global factors. The dots and the squares represent the displacements of the independent atoms in the lock-in phase at 100 K with respect to their positions in the basic structure.[20,39] It can be observed that the atomic modulation functions built from the harmonics obtained in the refinement according to the previous procedure describe very well the atomic positions in the lock-in phase. The discontinuous line in the figures represents the idealized distortion of Σ_2 symmetry obtained from the soliton model with a soliton density $n_s=0.4$, including the full Fourier series, instead of only the two refined harmonics. As expected, the dots and squares that represent the atomic displacements in the lock-in phase are located in the middle of the quasisteps in the atomic modulations, and their values agree very well with the values associated to these incipient steps.

These results confirm therefore the consistency of the experimental incommensurate structural modulation determined at 194 K and its description as a soliton configuration following the pattern predicted by a Landau-type approach with the structural data of the lock-in phase at 100 K determined by Quilichini and Pannetier.[20] Similar results are obtained when atomic positions in the lock-in phase at 115 K (Ref. 40) and at 146 K (Ref. 41) are considered.

VI. CONCLUSIONS

The experimental structure of Rb_2ZnCl_4 in its incommensurate phase just 2 K above the lock-in transition presents a highly anharmonic modulation. Synchrotron diffraction experiments have permitted to determine harmonics in the atomic modulations up to the fifth order. The observed anharmonicity follows a pattern that can be quantitatively compared and agrees very well with the soliton regime predicted by the Landau-type description of these incommensurate systems. The soliton density corresponding to the determined structure can be estimated to be 0.4, in agreement with results obtained with spectroscopic techniques.

ACKNOWLEDGMENTS

We would especially like to thank Vaclav Petricek for making modifications of his program JANA2000 that greatly helped our work. We would like also to thank Dr. H.-G. Krane for valuable suggestions concerning the synchrotron measurements. This work was supported by the TMR-Contract No. ERBFMGECT950059 of the European Community. K.F. acknowledges financial support by the Spanish Ministerio de Ciencia y Tecnología/Ministerio de Educación y Cultura.

*Author to whom correspondence should be addressed. Electronic address: ibon.aramburu@ehu.es

[1] *Incommensurate Phases in Dielectrics*, edited by R. Blinc and A. P. Levanyuk (North-Holland, Amsterdam, 1986), Vol. 1.
[2] *Incommensurate Phases in Dielectrics*, edited by R. Blinc and A. P. Levanyuk (North-Holland, Amsterdam, 1986), Vol. 2.
[3] H. Z. Cummins, Phys. Rep. **185**, 211 (1990).
[4] R. A. Cowley, Adv. Phys. **29**, 1 (1980), and references therein.
[5] R. Blinc, V. Rutar, B. Topic, F. Milia, and Th. Rasing, Phys. Rev. B **33**, 1721 (1986).
[6] W. Selke, Phys. Rep. **170**, 213 (1998).
[7] T. Janssen, O. Radulescu, and A. N. Rubtsov, Eur. Phys. J. B **29**, 85 (2002).
[8] B. Topic, U. Haeberlen, and R. Blinc, Phys. Rev. B **42**, 7790 (1990).
[9] H. Bestgen, Solid State Commun. **58**, 197 (1986).
[10] R. Blinc, B. Lozar, F. Milia, and R. Kind, J. Phys. C **17**, 241 (1984).
[11] M. Sylvia, S. Dantas, A. S. Chaves, R. Gazzinelli, and M. A. Pimenta, Ferroelectrics **105**, 165 (1990).
[12] M. B. Zapart, Phase Transitions **43**, 179 (1993).
[13] F. J. Zúñiga, G. Madariaga, W. A. Paciorek, J. M. Pérez-Mato, J. M. Ezpeleta, and I. Etxebarria, Acta Crystallogr., Sect. B: Struct. Sci. **B45**, 566 (1989).
[14] O. Hernández, M. Quilichini, J. M. Pérez-Mato, F. J. Zúñiga, M. Dusek, J.-M. Kiat, and J. M. Ezpeleta, Phys. Rev. B **60**, 7025 (1999).
[15] I. Aramburu, G. Madariaga, and J. M. Pérez-Mato, Phys. Rev. B **49**, 802 (1994).
[16] P. Prelovsek and R. Blinc, J. Phys. C **17**, 577 (1984).
[17] J. Petersson and E. Schneider, Z. Phys. B: Condens. Matter **61**, 33 (1985).
[18] R. Blinc, P. Prelovsek, A. Levstik, and C. Filipic, Phys. Rev. B **29**, 1508 (1984).
[19] M. P. Trubitsyn and T. M. Bochkova, Ferroelectrics **103**, 11 (1990).
[20] M. Quilichini and J. Pannetier, Acta Crystallogr., Sect. B: Struct. Sci. **B39**, 657 (1983).
[21] A. Hedoux, D. Grebille, J. Jaud, and G. Godefroy, Acta Crystallogr., Sect. B: Struct. Sci. **B45**, 370 (1989).
[22] A. Y. Babkevich and R. A. Cowley, J. Phys.: Condens. Matter **11**, 1639 (1999).
[23] J. M. Pérez-Mato and G. Madariaga, Solid State Commun. **58**, 105 (1986).
[24] S. R. Andrews and H. Mashiyama, J. Phys. C **16**, 4985 (1983).
[25] I. Aramburu, G. Madariaga, D. Grebille, J. M. Pérez-Mato, and T. Breczewski, J. Phys. I **7**, 371 (1997).
[26] M. Agirtmis, H. A. Farach, R. J. Creswick, and C. P. Poole, Jr., Ferroelectrics **300**, 33 (2004).
[27] I. Aramburu, G. Madariaga, and J. M. Pérez-Mato, Acta Crystallogr., Sect. A: Found. Crystallogr. **A53**, 334 (1997).
[28] V. Petříček and M. Dušek, JANA2000, Crystallographic Computing System, Institute of Physics, Academy of Science of the Czech Republic, Praha, Czech Republic, 2000.

[29] K. Itoh, A. Hinasada, H. Matsunaga, and E. Nakamura, J. Phys. Soc. Jpn. **52**, 664 (1983).
[30] I. Aramburu, G. Madariaga, and J. M. Pérez-Mato, J. Phys.: Condens. Matter **7**, 6187 (1995).
[31] J. M. Pérez-Mato, G. Madariaga, F. J. Zúñiga, and A. García Arribas, Acta Crystallogr., Sect. A: Found. Crystallogr. **A43**, 216 (1987).
[32] J. M. Pérez-Mato, G. Madariaga, and M. J. Tello, J. Phys. C **19**, 2613 (1986).
[33] For the sake of simplicity, in this section wave vectors are expressed within the usual solid state convention, with no explicit 2π factor, while in previous sections we use the usual crystallographic convention with this factor explicit.
[34] M. Iizumi, J. D. Axe, G. Shirane, and K. Shimaoka, Phys. Rev. B **15**, 4392 (1977).
[35] I. Etxebarria, J. M. Pérez-Mato, and G. Madariaga, Phys. Rev. B **46**, 2764 (1992).
[36] L. Palatinus, M. Amami, and S. van Smaalen, Acta Crystallogr., Sect. B: Struct. Sci. **B60**, 127 (2004).
[37] J. M. Pérez-Mato, F. Gaztelua, G. Madariaga, and M. J. Tello, J. Phys. C **19**, 1923 (1986).
[38] M. I. Aroyo and J. M. Pérez-Mato, Acta Crystallogr., Sect. A: Found. Crystallogr. **A54**, 19 (1998).
[39] J. M. Pérez-Mato, in *Methods of Structural Analysis of Modulated Structures and Quasicrystals*, edited by J. M. Pérez-Mato, F. J. Zúñiga, and G. Madariaga (World Scientific, Singapore, 1991), p. 117.
[40] F. Parisi and H. Bonadeo, Acta Crystallogr., Sect. A: Found. Crystallogr. **A53**, 286 (1997).
[41] K. Itoh, A. Hinasada, M. Daiki, and E. Nakamura, J. Phys. Soc. Jpn. **58**, 2070 (1989).